Surfzone bedform migration and sediment flux implications to large scale morphologic evolution

Wengrove, Meagan E.; de Schipper, Matthieu A.; Lippmann, Thomas C.; Foster, Diane L.

DOI
10.1016/j.geomorph.2022.108246

Publication date
2022

Document Version
Final published version

Published in
Geomorphology

Geomorphology 410 (2022) 108246

Contents lists available at ScienceDirect

Geomorphology

journal homepage: www.journals.elsevier.com/geomorphology

Surfzone bedform migration and sediment flux implications to large scale morphologic evolution

Meagan E. Wengrove [a,*], Matthieu A. de Schipper [b], Thomas C. Lippmann [c], Diane L. Foster [d]

[a] School of Civil and Construction Engineering, Oregon State University, 101 Kearney Hall, Corvallis, OR 97331, USA
[b] Faculty of Civil Engineering and Geosciences, Delft University of Technology, Stevinweg 1, Delft, 2628 CN, The Netherlands
[c] Department of Earth Sciences, University of New Hampshire, 24 Colovos Road, Durham, NH 03824, USA
[d] School of Marine Science and Ocean Engineering, University of New Hampshire, 8 College Road, Durham, NH 03824, USA

ARTICLE INFO

Keywords:
Sand ripples
Superimposed bedforms
Nearshore sediment transport
Bedform dynamics
Sandbar
Morphologic change
Surfzone

ABSTRACT

Field observations of small scale seabed morphology were obtained over 4 weeks at two locations separated 66 m along a cross-shore transect during the 2014 MEGAPEX Experiment conducted as part of the longer term Sand Engine mega-nourishment project along the North Sea Coast of The Netherlands. The seafloor was continuously covered by dynamic bedforms with amplitudes ranging 0.02–0.40 m and wavelengths ranging 0.20–2.5 m. Ripple migration rates were up to 3.6 m/h, dependent on the energy of the waves and currents. Under the assumption of bedload dominant transport, cross-shore and alongshore sediment volume flux by ripples was estimated from observations at the spatially separated imaging locations. The average and maximum ripple sediment volume flux was found to be 0.22 and 1.7 m^3/m/day, respectively, with larger fluxes during spring flood tides and storm wave conditions. The daily averaged fluxes were usually oriented about 30° north of shore-normal, moving in the same direction as a nearby transverse sandbar migration direction. Estimated gradients in the sediment flux within the surfzone were computed from bed level change measurements of the inner surfzone including a larger scale transverse sandbar measured from subsequent jetski surveys. We find that the estimated gradients in surfzone sediment flux are conceivably driven by small variations in the sediment flux driven by sand ripple migration, supported by our observations of ripple driven sediment flux at the two ripple imaging stations. A simple conceptual model is presented that shows how small scale bedforms may contribute to the growth and decay of larger scale bathymetric features, such as sandbars. Results suggest that sediment flux by small scale sand ripples and megaripples could significantly contribute to larger scale morphologic development in the surfzone.

1. Introduction

Sand ripples *O* (0.1 m to 10 m wavelength) superimposed on medium to large scale morphology *O* (10 m to 1000 m horizontal length) is characteristic of sub-aqueous environments (e.g., rivers, river inlets, tidal shoals, estuaries, and the coastal ocean). The influence of sand ripples on larger scale morphology (and vice versa) has historically been viewed through the lens of equilibrium and disequilibrium morphological theories, which pose that varying scales of superimposed bedforms simply coexist, but do not necessarily interact, evolution of each scale of bedform is viewed as independent from other scales (Allen and Collinson, 1974; Myrow et al., 2018). However, there is a body of geophysical observations that acknowledge the qualitative to quantitative potential for nonlinear dynamic feedback between scales of morphology (Off, 1963; Lippmann and Holman, 1990; Gallagher et al., 1998; Werner, 1999; Ashton et al., 2001; Venditti et al., 2005; Murray et al., 2009; Lefebvre et al., 2013; Doré et al., 2016; Jones and Traykovski, 2019). In rivers and inlets there is significant evidence for morphologic scale interactions (Dietrich and Smith, 1984; Dalrymple and Rhodes, 1995; Passchier and Kleinhans, 2005; Winter et al., 2008; Lefebvre et al., 2013). In estuaries and on shoals, megaripples *O* (1 m) have been shown to drive sand wave and dune *O* (250 m) migration despite the large difference in scale of these two morphological features (Dalrymple and Rhodes, 1995; Jones and Traykovski, 2019). At the beach, scale interactions are also found, where sandbar welding (the process whereby a sandbar migrates toward the coast and attaches to the

* Corresponding author.
E-mail address: meagan.wengrove@oregonstate.edu (M.E. Wengrove).

https://doi.org/10.1016/j.geomorph.2022.108246
Received 28 July 2021; Received in revised form 29 March 2022; Accepted 4 April 2022
Available online 22 April 2022

shoreline) can be a significant source of sediment to prograding shorelines (Bailard, 1981; Plant et al., 1999; Aagaard et al., 2004; Price and Ruessink, 2011; Ruggiero et al., 2016; Price et al., 2017).

The processes that drive beach evolution are inadequately understood (Hoefel and Elgar, 2003; Ludka et al., 2015; Ruggiero et al., 2016), especially in nearshore regions where sand ripples are ubiquitous (Clarke and Werner, 2004; Hay and Mudge, 2005). Established equilibrium coastal profile models generally poorly reproduce the beach shape in the surfzone when ripples and sandbars are dominant morphologic features (Dean, 1991; Clarke and Werner, 2004; Ludka et al., 2015). Moreover, coastal morphologic change models are shown to under-predict large-scale coastal adjustment in regions that are populated by dynamic sand ripples and sandbars (Terwindt and Wijnberg, 1991; Sherman, 1995; Brakenhoff et al., 2020). At present, coastal and riverine sediment transport formulations used in morphologic change models primarily characterize bedload transport due to the mobility of individual sand grains (Nielsen, 1992; Wengrove et al., 2019). Some transport formulations consider ripple influence, but only via a friction factor that modulates the shear stress or hydrodynamic power imposed from the flow to grains of sediment on the bed (e.g. Soulsby, 1997; Styles and Glenn, 2000; Soulsby and Clarke, 2005; Soulsby et al., 2012). Within the surfzone, observations show that bedforms (ripples and megaripples) often cover the seabed (Clarke and Werner, 2004; Becker et al., 2007), and ripples have been shown to affect both the magnitude and direction of sediment flux (Aagaard et al., 2001; Saulter et al., 2003; Hay and Mudge, 2005; van Rijn, 2007; Wengrove et al., 2018). Additionally, Dietrich and Smith (1984) showed bedload transport and transport due to ripple migration to be nearly the same magnitude in rivers and Doré et al. (2016) numerically showed that superimposed bedforms on a dune promote the decay of the dune crest in unidirectional flow.

The work presented herein supports the developing theory that superimposed bedforms contribute to larger scale sediment transport within the dynamic surfzone. We observe sediment volumetric flux caused by migrating sand ripples of O (0.2–2.5 m) in a mixed wave-current dominated inner surfzone to be consistent with the volumetric

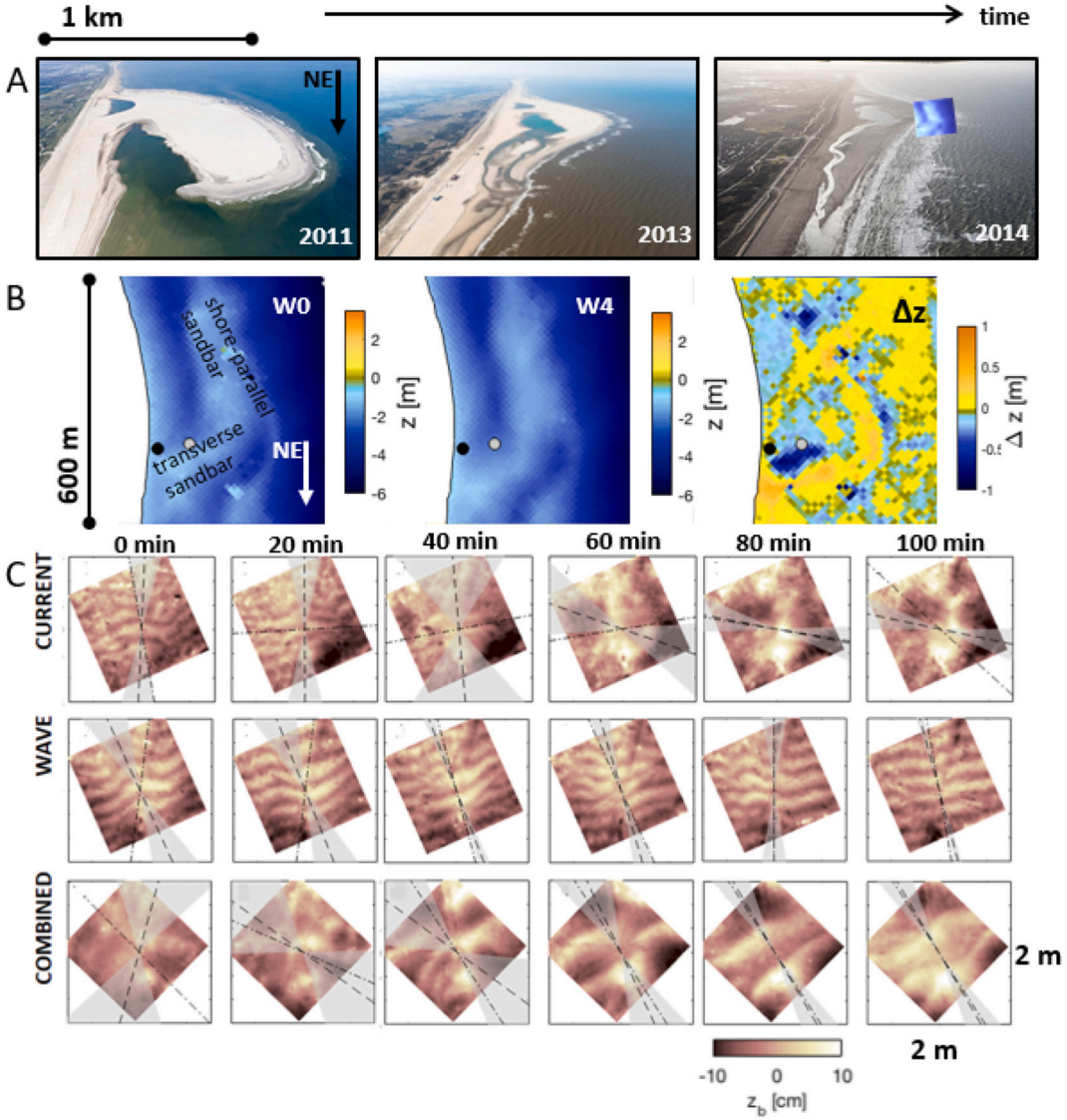

Fig. 1. Scales of morphology and their evolution through time at the Sand Engine. (a) large scale nourishment evolution (images from Joop van Houdt/Rijkswaterstaat). (b) medium scale transverse sandbar evolution from bathymetric surveys over a four week period (W0 to W4, top two panels) and respective change (bottom panel – blue erosion, orange accretion); black box highlights the transverse sandbar of interest and solid thin black curved line along the left-hand-side of each panel is the shoreline. (c) current, wave, and combined wave-current time series of spatial distribution of measured ripple elevation (z_b) as sampled at the sonar stations highlighted in (b) by black (shoreward) and grey (seaward) dots. Panel sets should be viewed from left to right and are forced by the indicated hydrodynamic condition to the left. Each set of observations were captured with a sampling rate of 20 min.

sand loss of the inner surfzone associated with a migrating shore-attached transverse sandbar. Quantifiable evidence of the importance of bedforms as an intermediate contributor to accretion and/or diffusion of larger scale morphologic features indicates a need for process based models to specify the contribution from ripple processes apart from traditional bedload and suspended load transport paramaterizations. Jones and Traykovski (2019) suggest a quantified and validated conceptual model that connects megaripple convergence and divergence to larger scale dune migration. Herein, we independently developed a similar conceptual model relevant to modulation of surfzone morphologies. It may be that modeling bedform kinematics as a physical process, rather than using a grain-by-grain assemblage of sediment transport, is a more representative method to parameterize the physics of superimposed bedforms in process based morphologic change models.

2. Observations

On sandy beaches there exists a spectrum of horizontal morphologic scales that range five orders of magnitude from 10^{-1}–10^{4} m. The largest scales of morphology are associated with the coastline, medium scales with sandbars, and smaller scales with sand ripples and megaripples. For the analysis presented herein, we utilize bathymetric field data that reveals morphologic evolution across a range of spatial and temporal scales obtained along the large sandy coastline of the Sand Engine in the Netherlands (Stive et al., 2013). We consider the largest morphologic scale in the system to be the curved Sand Engine coastline (Fig. 1). At the outermost protrusion of the Sand Engine, we use field observations of ripple migration to estimate the cross shore and the alongshore sediment volume flux along a cross-shore transect.

The curved Sand Engine mega-nourishment experimental project was installed in 2011 by depositing 21.5 million cubic meters of sand along a 2 km section of coast and extending 1 km into the North Sea (Fig. 1a upper panel). For context, the Sand Engine is a Building with Nature campaign, investigating if naturally existing waves and currents can push the added sand alongshore into erosive areas of the coast. The perturbation was predicted to diffuse over time and last for a period of over 20 years (whereas typical nourishments installed to protect the coast and create recreational beach width have a typical design lifespan of 4–5 years) (de Schipper et al., 2016).

The span of temporal and spatial scales of morphology present at the Sand Engine mega-nourishment system changes over periods ranging from minutes to years and spatial scales ranging from 10^{-2} to 10^{3} m (Fig. 1) (de Schipper et al., 2016; Rutten et al., 2018; Wengrove et al., 2019). On the largest scales considered the morphology of the Sand Engine evolved significantly, moving millions of cubic meters of sand (Fig. 1a, lower panel) (Stive et al., 2013; Huisman et al.(2016), de Schipper et al., 2016; Radermacher et al., 2017; Wengrove et al., 2018; Roest et al., 2021). At medium scales, jet-ski surveys were used to observe morphologic change of the local shore-parallel and transverse sandbars in 2014 (Fig. 1). The transverse sandbars are generally 1.5 m in height and approximately 100 m wide in the alongshore direction, and evolve over periods of days to months (Fig. 1b). Over a period of just four weeks in 2014 the transverse sandbar (indicated in Fig. 1b) migrated 50 m toward the northeast (Fig. 1b, lower panel). On the small scale, two sonar imaging stations offset by 66 m in the cross-shore (shore-normal) direction were deployed in 2014 (coinciding with the jet-ski surveys) to simultaneously measure ripple-scale bedform evolution (Fig. 1b, 3b). Our work investigates the possible connection between the migrating sand ripples in the surfzone (Fig. 1c) to the concomitant evolution of the transverse migrating sandbar (Fig. 1b).

3. Methods

3.1. Field measurements

Observations were collected in 2014 during a four week long field experiment from 23 September (day of year (DOY) 256) to 18 October (DOY 291). Two large-scale bathymetric surveys were obtained using a jet-ski equipped with an single-beam echo sounder and differential GPS positioning on 23 Sept. and 18 Oct. (DOY 266 and 291), and subsequently used to estimate surfzone change and sandbar evolution. Small-scale ripples were observed with two imaging stations positioned at the tip of the Sand Engine using pencil beam rotary sonars (Wengrove et al., 2017). The sonars were deployed offset in the cross-shore direction by 66 m between the seaward sandbar (the sandbar was 50 m further seaward than the outer sonar station, S2) and the shoreline (the shoreline was 20 m further shoreward than the inner sonar station, S1). Additionally, the stations were positioned southwest of a migrating transverse sandbar. The inner ripple imaging station will be referred to as S1 and the outer as S2. The alongshore direction was defined based on the orientation of the Delfland coastline without the mega-perturbation. The S2 sonar station was deployed for 2 weeks (DOY 275 to 291), while S1 was deployed for 4 weeks (DOY 269 to 296). Generally, waves were breaking at the S1 sonar station closest to shore, especially during low tide; while at the S2 sonar station, waves were reshoaling after breaking on the offshore shore parallel sandbar (Wengrove et al., 2017, 2018, 2019). Details of the experimental setup and observations of ripple transformation and forcing conditions are included in Supplementary Material A.

3.2. Ripple driven transport

Ripples have been previously observed and analyzed for changes in ripple wavelength, height, migration rate, and migration direction (Fig. 1c) (Wengrove et al., 2018, 2019). Following (Traykovski et al., 1999), an estimate of sediment flux mobilized by ripple migration can be obtained using the bedload sediment flux associated with migrating ripples,

$$q_{ripple} = \frac{1}{2} n V_{mig} \eta \tag{1}$$

where V_{mig} is the ripple migration rate, η is the ripple height, and n is an empirical sediment packing factor (taken as 0.7). V_{mig} is calculated from two-dimensional (2D) cross correlation or motion estimator process applied to pairs of sonar images sampled 20 min apart, and η is calculated from 2D spectra of individual images (see Supplementary Material B). Three example time series of successive images over a 100 min period illustrate the dynamic ripple adjustment to wave dominant and current dominant flow conditions (Fig. 1c). The combined wave-current conditions yielded (by far) the most mobile ripples (Fig. 1c, (Wengrove et al., 2018)).

The error in sediment flux estimated by propagating quadrature error is placed on estimates of ripple height and migration rates. For ripple heights, a chi-square distribution was used to determine the standard deviation on the 2D ripple height variance. The maximum error for the entire time series was 0.01 m. Estimated standard deviation was placed on ripple migration rates based on two methods. The first was based on the variance explained using 2D cross correlation methods, in which the maximum error in V_{mig} of 0.3 cm/min is found by considering the error of the migration rate given by twice the smallest spatial resolution of the sonar over a 20-min window $\frac{(2\times 0.03\mathrm{m})}{(20 min)}$. The second was based on the correlation roll off error at the point where the correlation became less than 60%, and was also found to be 0.3 cm/min. The error in the packing factor, n, was taken to be 0.7 ± 0.05 based on variability in estimates of n in literature for bed packing and ripple shape (Sleath, 1984). Total propagated error was estimated by assuming independent variables in quadrature using a standard error approach,

$$q_{ripple_{error}} = \sqrt{\left[(n_{error}/n)^2 + (\eta_{error}/\eta)^2 + \left(V_{mig_{error}}\right) \Big/ \left(V_{mig}\right)^2 \right] q_{ripple}} \tag{2}$$

The daily maximum error was found by integrating over a day.

Maximum error was ±0.1 m^3/m/day and is indicated by vertical error bars in Fig. 3b. Miss-alignment of the sonar would lead to error in estimates of q_x (cross shore) and q_y (alongshore) from ripple driven sediment flux; we estimate those errors to be at ±0.03 m^3/m/day for a maximum 10° miss-alignment.

3.3. Analysis of large-scale transverse sandbar

Jet-ski surveys were used to observe morphologic change of the local shore parallel and transverse sandbars (Figs. 1, 3, 4). The location of the bathymetric surveys is at the tip of the Sand Engine, shown in the lower panel of Fig. 1. Surveys were referenced to a local datum and water level fluctuations (waves, infragravity motions and tide) were compensated by RTK-GPS measurements of the jetski. Errors in the obtained bed elevations originate from the RTK GPS system, pitch/roll of the jetski, bed detection and sound propagation speed used in the sounder (MacMahan, 2001). Comparisons between surveys made on different days were accomplished by removing bias between surveys and accounting for systematic depth errors (e.g. variable mounting of the GPS antenna, salinity fluctuations). We removed bias by normalizing surveys to elevations in regions with little to no morphologic change (i.e., offshore), the approach is more conservative than other approaches used to reference multiple surveys to the same level. Although the bias normalization should have accounted for inherent depth errors, to be conservative, we accounted for inherent depth bias error from the jet-ski surveys by estimating confidence on survey elevations as 0.5% of the depth with an added 3 cm offset due to systematic errors in setup (de Zeeuw et al., 2016). Hence bias in bed elevations range from 3 cm near the beach and increased to 6 cm at the deepest extent of the survey region. The change in depth error between two jet-ski surveys was estimated again using the quadrature error for subtracted quantities approach for each set of differenced surveys.

3.4. Sediment flux and bed level change

The sediment flux and bed level change are related using the sediment continuity equation

$$\frac{dz_b}{dt} = -\frac{1}{n}\nabla q \tag{3}$$

where n is the sediment packing, ∇q is the gradient in sediment flux, and dz_b/dt is the change in the bed level over a defined period of time, t.

The sediment flux per meter of sandbar length (q_{sb}) is estimated with the migration of the transverse sandbar by

$$q_{sb} = \frac{1}{2} n \eta_{sb} V_{mig_{sb}} \tag{4}$$

where η_{sb} is the sandbar height and $V_{mig_{sb}}$ is the sandbar migration rate.

4. Results

4.1. Ripple dynamics

The hydrodynamic forcing was at times very strong, with wave orbital velocities near 0.6 m/s and current velocities near 0.7 m/s (Fig. 2). The median grain size within the inner bar region was between 250 μm and 400 μm, with most sediments closest to 350 μm (Huisman et al., 2016). Fig. 2b,c show the combined wave current Shields parameter (for characterizing bedload transport) and Rouse number (for characterizing suspended load transport) for the most common grain size 350 μm and the minimum grain size (250 μm) at the tip of the Sand Engine. Shields parameters ranging between 0.05 and 0.7 and Rouse numbers primarily above 2.5 indicate conditions dominated by bedload transport for a grain size of 350 μm, and mixed load transport for the minimum grain size of 250 μm. Thus, during the periods of time

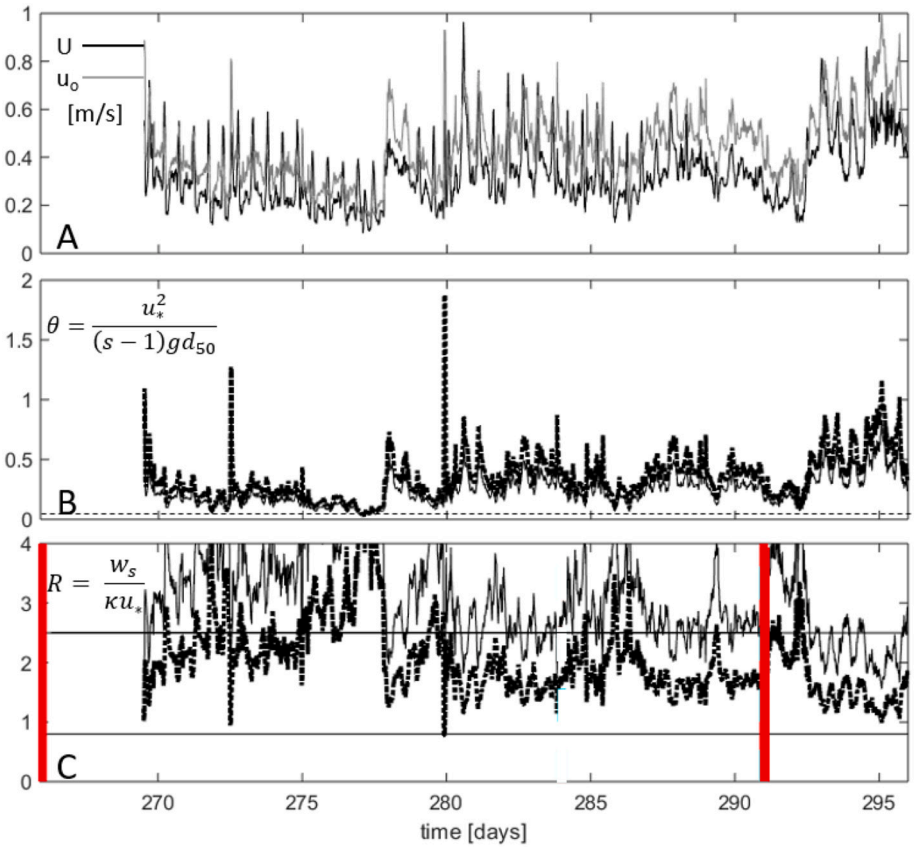

Fig. 2. Experimental campaign wave (u_o) and mean current (U) hydrodynamic conditions (A) and sediment transport characterization using the combined wave-current Shields parameter (B) and Rouse number (C). Shields parameter threshold for incipient motion is 0.05 indicated by the thin dashed line in (B), sheet flow occurs at a Shields parameter of approximately 0.8. Suspended sediment transport occurs at a Rouse number of 2.5 and lower, wash load occurs at a Rouse number of 0.8 and lower for that grain size, both thresholds are plotted as solid black lines in (C). Both the Shields and Rouse numbers are plotted for a median grain size of 350 μm (thin) and 250 μm (dotted bold) (middle). The red vertical lines indicate analysis period DOY 266–291, respectively. u_* is the friction velocity, s is the specific gravity of the sediment, g is the acceleration due to gravity, d_{50} is the particle median grain size, w_s is the settling velocity for the particle median grain size, and κ is the von Karman coefficient defined as 0.4.

considered for the following analysis, bedload transport is assumed to be the significant contributor to the total load. For the period DOY 275–291, sediment of grain size 250 μm and coarser are estimated to be mobile for the full period (Fig. 2b), the 250 μm grain size reaches the threshold for suspension nearly 100% of the time and the 350 μm grain size reaches the threshold for suspension 10% of the time, neither approach wash load (Fig. 2c). For the full period (DOY 266–291) the 250 μm grain size sediment and coarser are estimated to be mobile (Fig. 2b), while the 250 μm grain size reaches the threshold for suspension approximately 80% of the time and the 350 μm grain size reaches the threshold for suspension only 15% of the time, neither approach wash load (Fig. 2c). As such, the most common grain size (350 μm) was mobile in the regime of bedload transport for nearly 90% of the measurement period (ideal conditions for bedload transport), while the minimum grain size (250 μm) was estimated to be moving in the regime of bedload 50% of the time during ebb tide and suspended load during flood tide.

Shields parameters ranging between 0.1 and 0.6 suggest ripple driven transport in sandy bottom environments. The cross-shore and alongshore daily averaged sediment flux time series was estimated for each ripple imaging station using observations of ripple migration and migration direction (shown with a time series in Fig. 3a and with vectors in Fig. 3b) (Wengrove et al., 2018). Sand ripple transformation at the seaward tip of the Sand Engine was observed to range in wavelength between 0.12 and 2.5 m with heights between 0.02 and 0.4 m and migration rates up to 3.6 m/h dependent on the hydrodynamic energy in the overlying waves and currents (Fig. 1c) (Wengrove et al., 2017, 2018, 2019). Over the course of the experiment (between DOY 275–291), the average and volumetric sediment flux per unit width per day of sand transported by observed ripple migration was found to be 0.19 m^3/m/day (S1) and 0.24 m^3/m/day (S2), the average between the two sites was then 0.22 m^3/m/day, and when broken into cross- and alongshore components, was on average 0.20 m^3/m/day in the cross shore and 0.11 m^3/m/day in the alongshore. The maximum observed daily averaged sediment flux during the experiment occurred at S1 on DOY 295 with a flux rate of 1.7 m^3/m/day (Fig. 3a). The daily averaged sediment flux was directed just northeast (30°) of shore normal for most days (Fig. 3a color, 3b vectors). Larger flux rates occurred during spring flood tides (DOY 266, 281, 296) and during storm conditions (DOY 278, 280, 287, 294). Both stations follow the same temporal variations with respect to magnitude and direction of sediment flux, with the exception of the storm event between DOY 280–283, during which the wave driven alongshore current was stronger at S2 (Fig. 3b).

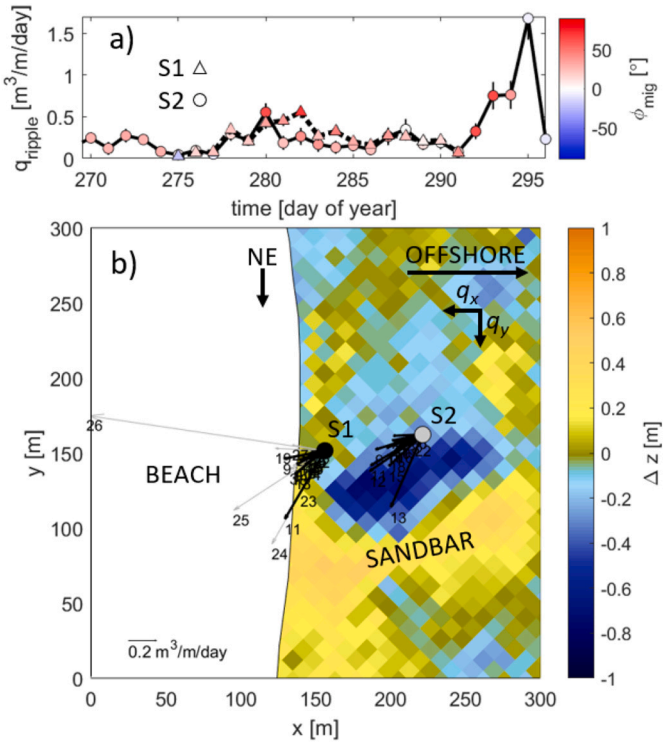

Fig. 3. Ripple driven sediment flux observed at the S1 and S2 sonar stations. (a) Time series of daily averaged magnitude of the ripple sediment flux colored by the ripple migration direction, where +90° is directed alongshore toward the northeast. Circles indicate the S1 sonar station and the triangles indicate the S2 sonar station. Storms occurred on DOY 278, 280, 287, and 294. Quadrature error bars are plotted as vertical lines. (b) Bathymetric difference survey between DOY 266 and DOY 291 overlaid with daily averaged sediment flux vectors for each sonar station S1 and S2. Vectors numbered according to time position in top panels; 1 being the first point in the time series. The black vectors highlight the period of time when both sonar stations were deployed, and the grey vectors on the S1 station show the remainder of measurements for the deployment. The 0.2 m^3/m/day scale bar in the lower left corner indicates transport magnitude relevant for interpreting the plotted sediment flux vectors for q_{ripple}.

4.2. Ripple driven transport compared to surfzone volumetric change

The jetski survey data was used to estimate surfzone volumetric change between the survey pair by taking the difference between the bathymetric survey pair between DOY 266–291 (Fig. 3b). To put the bathymetric change observations in terms of a quantity that we can compare with observations of ripple driven sediment flux we use the sediment continuity equation (Eq. (3)). The average gradient in sediment flux needed ($\nabla\overline{q_{est}}$) to drive the observed bathymetric change observations (Δz_b), is defined as

$$\nabla\overline{q_{est}} = -n\Delta z_b dxdy/dt \tag{5}$$

where $dxdy$ is taken to be 1 m^2 (to compare with $\overline{q_{ripple}}$) and dt is the time in days between surveys. Fig. 4 shows the estimated (or derived) gradient in sediment flux from the changes in observed bathymetry for the two sets of survey pairs. The average ripple driven sediment flux at S1 and S2 was computed over the duration of time S1 and S2 were deployed synchronously (DOY 275–291, Fig. 3a). Note, unfortunately we do not have a survey collected on DOY 275, so the average ripple driven sediment flux is computed over a shorter period of time than the

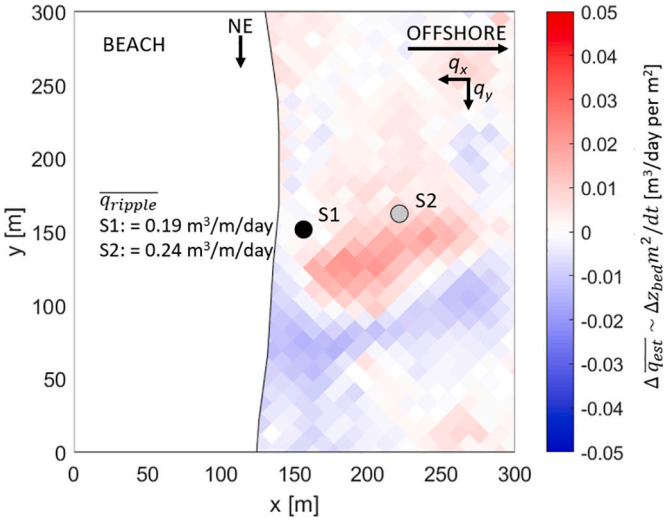

Fig. 4. Estimated average gradients in sediment flux from changes in observed bathymetry for survey pair between DOY 266–291. Red colors represent erosion of sediment, while blue colors represent accretion of sediment. The observed sediment flux from the ripple imaging stations (S1 and S2) is labeled in the figure.

gradient in estimated sediment flux, but still with representative calm and storm conditions.

The estimated gradient in sediment flux from the survey pair between DOY 266–291 (Fig. 4), shows that in the cross shore position where the ripple imaging stations were located, there was a moderately erosive derived gradient in sediment flux. We also observe that in the region of transverse sandbar migration there were areas that were more erosive and areas that were more accretive. If we compare the observations of average ripple driven sediment flux to the estimated gradient in sediment flux from bed level change, we see that on average $\overline{q_{ripple}}$ would only need to change less than 0.02 m^3/day (i.e., less than ±10% of the observed $\overline{q_{ripple}}$ to accommodate bathymetric change across the transverse sandbar. As such, if ripples drove the observed bed level changes around the transverse sandbar, the ripple volume and/or migration speed of the ripples would need to be spatially dynamic, creating zones of higher sediment flux convergence and divergence. In erosive region near the sandbar, the average ripple sediment flux would need to be larger than that observed at S1 and S2, and in the accretive region the average ripple driven sediment flux would need to be smaller than that observed at S1 and S2. The estimated needed sediment flux divergences are not unreasonable for the system. Fig. 3a shows that on DOY 282, there is a divergence of approximately 0.3 m^3/m/day between the S1 and S2 observations of ripple driven sediment flux. Other observations in literature show that the divergence magnitude suggested is adequately reasonable for sandy systems (e.g., Jones and Traykovski (2019)). Of course, other mechanisms of sediment flux in the surfzone are also conceivable. In summary, the observed ripple driven sediment flux are large in magnitude compared to the derived gradients in sediment flux needed to drive surfzone bathymetric change. As such, our results feasibly suggest that sand ripple driven sediment flux is an important contributor to surfzone bathymetric change.

4.3. Ripple driven transport compared to sandbar migration

Ripple driven transport can be put into context with large scale estimates of sediment transport derived from measurements of the migration of the sandbar (Orzech et al., 2010). As the sandbar migrated along and toward the shore (Fig. 1b, Fig. 3), approximately $q_{sb} = 1.05$ m^3/m/day of sand was transported across the bar crest (the migration rate of the sandbar was approximately $V_{migsb} = 2$m/day, the sandbar height ≈ 1.5 m, Eq. (4)). The sandbar transport rate was calculated from successive bathymetric surveys obtained between DOY 266–291. We observed the transverse sandbar to migrate alongshore, while also accumulating sediment along its shoreward side (Figs. 1b, 3b).

Since the sandbar migration rate was only estimated in the alongshore direction, we compare relative magnitudes of alongshore sediment flux between the transverse sandbar (1.05 m^3/m/day) and the sand ripples (0.11 m^3/m/day). We find that the ripple driven sediment flux measured to the southwest of the northeasterly migrating transverse sandbar could only account for 10% of the net sediment transport associated with the alongshore transverse sandbar migration. The hydrodynamics everywhere along the bar are likely not the same as at the imaging stations, and thus the implicit assumption of ripple similitude along the transverse bar likely results in over- or under-prediction of the net transport volume. The sandbar not only migrated, it also changed volume during its evolution. The only way to estimate the true contribution of ripples to sandbar translation and growth or decay is by closing the sediment budget and preforming a sediment convergence/divergence analysis for sand entering into and leaving from the sandbar control area. Wengrove et al. (2018, 2019) show that at times ripples at the field site were subject to growth and shrinking in volume as they migrate, such that ripples can pick up and deposit sediment in the control area. Both concepts lead to our conceptual model for how sand ripples may aid in the growth and decay of sandbars.

5. Discussion

5.1. Conceptual model for sand ripples aiding in the growth and decay of sandbars

We consider a simple idealized sandbar as it migrates (Fig. 5a). The net change in sand volume, ΔV_{sb}, per unit planar area, A_{sb}, of a migrating sandbar equals the net bed level change, Δz_b,

$$\frac{\Delta V_{sb}}{A_{sb}} = \Delta z_b \tag{6}$$

where $\Delta V_{sb} = f(q_b, q_s)$, such that the change in sandbar volume per unit planar area (change in bed level) is a function of the bedload (q_b) and suspended load (q_s) sediment transport gradients over the sandbar area. We can evaluate the net bed level change, Δz_b, for cases where spatial changes in small scale sand ripples are dominant by,

$$\Delta z_b = \frac{\Delta V_{sb}}{A_{sb}} = n \int \frac{dq_{ripple}}{dl} dt \pm P \tag{7}$$

The first term on the right-hand-side is the time integrated ripple flux divergence and arises from the variability introduced by ripple migration over a given time interval, where dq_{ripple} is the net volumetric change in transport rate per unit cross-flux distance from migrating ripples separated in space by dl. When ripples migrate the migration is accomplished partially due to suspended load and partially due to bedload processes of sediment transport, though predominantly bedload driven, suspended sediments advected from ripples generally stay within the ripple system. As such q_{ripple} can be composed of both bedload and suspended load components. The simple model shows that migrating and transforming small-scale ripples can influence morphology evolving on longer time and length scales. The migrating

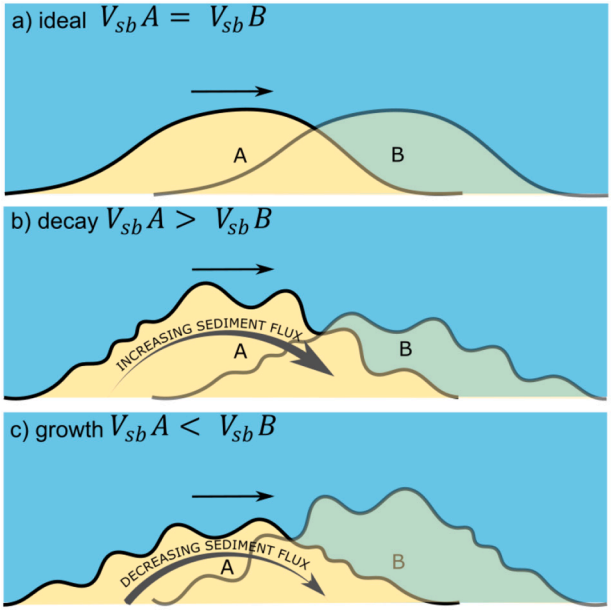

Fig. 5. Conceptual model showing influence of small-scale morphology on the transformation of larger scale morphology outlined as Eq. (5). A is the initial sandbar profile; B is the projected sandbar transformation at an arbitrary time in the future. (a) sandbar migration omitting changes in ripple induced sediment fluxes; the sandbar migrates but does not change shape. (b) condition leading to sandbar decay; ripples take sand away as they migrate over the sandbar. (c) condition leading to sandbar growth; ripples leave sand behind as they migrate over the sandbar. The arrows indicate the net transport direction. Ripple size is exaggerated for conceptual understanding with respect to sandbar size. Both (b) and (c) assume that term P in Eq. (5) is small. V_sb is the sandbar volume.

ripples may remove sediment from the sandbar under increasing sediment flux in the direction of ripple migration (Fig. 5b) or may add sediment to the sandbar under decreasing fluxes (Fig. 5c). The second term, P, accounts for any other transport process that may increase or decrease the volume of the sandbar during migration (e.g. sheet flow, sediment bypassing and deposition). It is our hypothesis that the transverse sandbar migration and growth/decay could be described at least in part by the conceptual model driven by ripple sediment flux; however, the hypothesis is only supported by our quantitative observations, but is yet to be proven.

5.2. Context and application of results

Observations of sand ripple geometric adjustment and migration in changing hydrodynamic conditions have been observed in the surfzone, tidally driven inlets and shoals, rivers, and laboratories. Dietrich and Smith (1984) show that sediment transport driven by sand ripple migration accounts for observed bed level change in riverine environments. Aagaard et al. (2001) show that sediment transport due to megaripples on a barred beach during the passing of a storm contribute a non-insignificant amount to the total bed level change of the beach. Jones and Traykovski (2019) show that megaripple transport is essential for the migration of sandwaves in a tidally dominated shoal environment. Our effort complements the results of the three aforementioned studies by 1) examining the influence that ripple and megaripple transport has on bed level change in the surfzone, and 2) examining the potential relationship between the small scale to medium scale geometric roughness adjustment in the surfzone through a conceptual model. The basis of our conceptual model is the same as that of Jones and Traykovski (2019), where they use the time integrated sediment continuity equation (Exner equation) with a substitution for ripple driven sediment flux to show that the sandwave migration rate and the change in sandwave elevation measured from bathymetric surveys is the same as that estimated from ripple convergence and divergence measurements. Although we could not calculate sediment convergence and divergence because of limitations in our observational array, we hypothesize that convergence and divergence of megaripples also significantly contribute to the change in shape and migration of the transverse bar in the surfzone and its multidirectional flows. The overall observed bedlevel change in the surfzone is consistent with observations of the estimated change due to spatially and temporally integrated ripple and megaripple transport over the period of observation.

Results are applicable to any medium to large scale geomorphic feature where migrating smaller scale ripples exist as part of a larger system. In our study and in the study of Jones and Traykovski (2019), hydrodynamic energy is mild to moderately high during the observational periods. In both studies bedlevel change can be nearly fully accounted for by ripple migration. During more energetic storms megaripple migration convergence and divergence may be less important for system change, but still a significant contributor as shown by Aagaard et al. (2001). Our observations focused on the bedlevel change and migration of a transverse sandbar in the inner surfzone where longshore and tidally driven currents are nearly as important as wave hydrodynamics. Ripple and megaripple dynamics also likely contribute to shore parallel bar dynamics.

Our results and the results of others suggest that process based model accuracy should improve with 1) inclusion of parameterizations for specific ripple and megaripple transport mechanics instead of the present parameterizations that divide bedload and suspended load transport as independent processes and 2) inclusion of convergence and divergence adjustment relationships between scales of morphology by accounting for ripple convergence influence on sandbars/sandwave morphodynamics and by accounting for ripple adjustment as a function of relative location of the ripples on the larger scale morphology.

6. Conclusion

Detailed observations of small-scale sand ripples and surfzone bathymetric evolution were acquired and analyzed to investigate the link between ripple mechanics and surfzone sediment transport. Field data supports the hypothesis that small-scale sand ripples could contribute significantly to larger scale bathymetric change in the surfzone under mild to moderately high hydrodynamic energy. Sand from the sand ripples and megaripples migrated both onshore to the beach and alongshore in the direction of the migration of a local transverse sandbar. A simple conceptual model shows how sand ripples can feed or erode larger surfzone morphology. Through field measurements, we show that the estimated gradient in sediment flux from bed level change measurements between a pair of jetski bathymetric surveys within the surfzone are reasonable values for divergence driven by ripple driven sediment flux in the surfzone. The conceptual model outlined as part of our study should be tested more robustly through tailored field and laboratory experiments. Our results are consistent with those in rivers (Dietrich and Smith, 1984), tidally dominated shoals (Jones and Traykovski, 2019) and the inter-tidal area (Aagaard et al., 2001), which suggest that sediment transport patterns observed through superimposed sand ripple migration and growth of larger morphologic features may contribute to larger scale patterns of net morphologic change. Results of our study and others encourage process based morphodynamic evolution models to strive to consider superimposed ripple dynamics as contributors to the evolution of large morphologic features. Active ripple dynamics should be considered as an important contributor to littoral and riverine morphodynamic evolution.

Declaration of competing interest

The authors declare that they have no known competing financial interests or personal relationships that could have appeared to influence the work reported in this paper.

Acknowledgements

We would like to acknowledge the team of graduate students, technicians, and faculty members from multiple countries and institutions who contributed to the Sand Engine experiment MEGAPEX. MEGAPEX was funded through NWO grant 12686, Nature Coast, and ERC Advance grant 91206, NEMO. The UNH contribution to MegaPEX was funded by the PADI Foundation. MEW was supported by the U.S. Department of Defense NDSEG fellowship. DLF was funded by NSF grant number 1135026. TCL was funded under ONR contract number N00014-14-1-0557. MdS was supported by NWO grant 15058, Feeding Starved Coasts by Morphological Diffusivity. We also would like to thank the reviewer contributions to clarity of the manuscript.

Appendix A. Supplementary data

Supplementary data to this article can be found online at https://doi.org/10.1016/j.geomorph.2022.108246.

References

Aagaard, T., Greenwood, B., Nielsen, J., 2001. Bed level changes and megaripple migration on a barred beach. J. Coast. Res. 110–116.
Aagaard, T., Davidson-Arnott, R., Greenwood, B., Nielsen, J., 2004. Sediment supply from shoreface to dunes: linking sediment transport measurements and long-term morphological evolution. Geomorphology 60, 205–224.
Allen, J., Collinson, J., 1974. The superimposition and classification of dunes formed by unidirectional aqueous flows. Sediment. Geol. 12, 169–178.
Ashton, A., Murray, A.B., Arnoult, O., 2001. Formation of coastline features by large-scale instabilities induced by high-angle waves. Nature 414, 296–300.
Bailard, J.A., 1981. An energetics total load sediment transport model for a plane sloping beach. J. Geophys. Res. Oceans 86, 10938–10954.

Becker, J., Firing, Y., Aucan, J., Holman, R., Merrifield, M., Pawlak, G., 2007. Video-based observations of nearshore sand ripples and ripple migration. J. Geophys. Res. Oceans 112.
Brakenhoff, L., Schrijvershof, R., Van Der Werf, J., Grasmeijer, B., Ruessink, G., Van Der Vegt, M., 2020. From ripples to large-scale sand transport: the effects of bedform-related roughness on hydrodynamics and sediment transport patterns in delft3d. J. Mar. Sci. Eng. 8, 892.
Clarke, L., Werner, B., 2004. Tidally modulated occurrence of megaripples in a saturated surf zone. J. Geophys. Res. Oceans 109.
Dalrymple, R.W., Rhodes, R.N., 1995. Estuarine dunes and bars. In: Developments in Sedimentology, 53. Elsevier, pp. 359–422.
de Schipper, M.A., de Vries, S., Ruessink, G., de Zeeuw, R.C., Rutten, J., van Gelder-Maas, C., Stive, M.J., 2016. Initial spreading of a mega feeder nourishment: Observations of the sand engine pilot project. Coast. Eng. 111, 23–38.
de Zeeuw, R., de Schipper, M.A., Tonnon, P.K., van der Valk, B., 2016. Morfologische ontwikkeling van de zandmotor pilot in de periode 2 tot 4,5 jaar na aanlegtechnical report. In: Shore Monitoring and Research.
Dean, R.G., 1991. Equilibrium beach profiles: characteristics and applications. J. Coast. Res. 53–84.
Dietrich, W.E., Smith, J.D., 1984. Bed load transport in a river meander. Water Resour. Res. 20, 1355–1380.
Doré, A., Bonneton, P., Marieu, V., Garlan, T., 2016. Numerical modeling of subaqueous sand dune morphodynamics. J. Geophys. Res. Earth Surf. 121, 565–587.
Gallagher, E.L., Elgar, S., Thornton, E.B., 1998. Megaripple migration in a natural surf zone. Nature 394, 165–168.
Hay, A.E., Mudge, T., 2005. Principal bed states during sandyduck97: occurrence, spectral anisotropy, and the bed state storm cycle. J. Geophys. Res. Oceans 110.
Hoefel, F., Elgar, S., 2003. Wave-induced sediment transport and sandbar migration. Science 299, 1885–1887.
Huisman, B., De Schipper, M., Ruessink, B., 2016. Sediment sorting at the sand motor at storm and annual time scales. Mar. Geol. 381, 209–226.
Jones, K.R., Traykovski, P., 2019. Interaction of superimposed megaripples and dunes in a tidally energetic environment. J. Coast. Res. 35, 948–958.
Lefebvre, A., Ernstsen, V.B., Winter, C., 2013. Estimation of roughness lengths and flow separation over compound bedforms in a natural-tidal inlet. Cont. Shelf Res. 61, 98–111.
Lippmann, T., Holman, R., 1990. The spatial and temporal variability of sand bar morphology. J. Geophys. Res. Oceans 95, 11575–11590.
Ludka, B., Guza, R., O'Reilly, W., Yates, M., 2015. Field evidence of beach profile evolution toward equilibrium. J. Geophys. Res. Oceans 120, 7574–7597.
MacMahan, J., 2001. Hydrographic surveying from personal watercraft. J. Surv. Eng. 127, 12–24.
Murray, A.B., Lazarus, E., Ashton, A., Baas, A., Coco, G., Coulthard, T., Fonstad, M., Haff, P., McNamara, D., Paola, C., et al., 2009. Geomorphology, complexity, and the emerging science of the earth's surface. Geomorphology 103, 496–505.
Myrow, P.M., Jerolmack, D.J., Perron, J.T., 2018. Bedform disequilibrium. J. Sediment. Res. 88, 1096–1113.
Nielsen, P., 1992. Coastal bottom boundary layers and sediment transport. World Scientific 4.
Off, T., 1963. Rhythmic linear sand bodies caused by tidal currents. AAPG Bull. 47, 324–341.
Orzech, M.D., Thornton, E.B., MacMahan, J.H., O'Reilly, W.C., Stanton, T.P., 2010. Alongshore rip channel migration and sediment transport. Mar. Geol. 271, 278–291.
Passchier, S., Kleinhans, M., 2005. Observations of sand waves, megaripples, and hummocks in the dutch coastal area and their relation to currents and combined flow conditions. J. Geophys. Res. Earth Surf. 110.
Plant, N., Holman, R., Freilich, M., Birkemeier, W., 1999. A simple model for interannual sandbar behavior. J. Geophys. Res. Oceans 104, 15755–15776.
Price, T., Ruessink, B., 2011. State dynamics of a double sandbar system. Cont. Shelf Res. 31, 659–674.
Price, T., van Kuik, N., de Wit, L., Dionsio António, S., Ruessink, B., 2017. Shoreward propagating accretionary waves (spaws): observations from a multiple sandbar system. Proc. Coast. Dyn. 2017, 1081–1089.
Radermacher, M., de Schipper, M.A., Swinkels, C., MacMahan, J.H., Reniers, A.J., 2017. Tidal flow separation at protruding beach nourishments. J. Geophys. Res. Oceans 122, 63–79.
Roest, B., de Vries, S., de Schipper, M., Aarninkhof, S., 2021. Observed changes of a mega feeder nourishment in a coastal cell: five years of sand engine morphodynamics. J. Mar. Sci. Eng. 9, 37.
Ruggiero, P., Kaminsky, G.M., Gelfenbaum, G., Cohn, N., 2016. Morphodynamics of prograding beaches: a synthesis of seasonal-to century-scale observations of the Columbia river littoral cell. Mar. Geol. 376, 51–68.
Rutten, J., Ruessink, B., Price, T., 2018. Observations on sandbar behaviour along a man-made curved coast. Earth Surf. Process. Landf. 43, 134–149.
Saulter, A., Russell, P., Gallagher, E., Miles, J., 2003. Observations of bed level change in a saturated surf zone. J. Geophys. Res. Oceans 108.
Sherman, D.J., 1995. Problems of scale in the modeling and interpretation of coastal dunes. Mar. Geol. 124, 339–349.
Sleath, J.F., 1984. Sea Bed Mechanics.
Soulsby, R., 1997. Dynamics of Marine Sands.
Soulsby, R., Clarke, S., 2005. Bed Shear-stress Under Combined Waves and Currents on Smooth and Rough Beds tr 137.
Soulsby, R., Whitehouse, R., Marten, K., 2012. Prediction of time-evolving sand ripples in shelf seas. Cont. Shelf Res. 38, 47–62.
Stive, M.J., De Schipper, M.A., Luijendijk, A.P., Aarninkhof, S.G., van Gelder-Maas, C., Thiel, Van, de Vries, J.S., De Vries, S., Henriquez, M., Marx, S., Ranasinghe, R., 2013. A new alternative to saving our beaches from sea-level rise: the sand engine. J. Coast. Res. 29, 1001–1008.
Styles, R., Glenn, S.M., 2000. Modeling stratified wave and current bottom boundary layers on the continental shelf. J. Geophys. Res. Oceans 105, 24119–24139.
Terwindt, J.H., Wijnberg, K.M., 1991. Thoughts on large scale coastal behavior. Coast. Sediments ASCE. 1476–1487.
Traykovski, P., Hay, A.E., Irish, J.D., Lynch, J.F., 1999. Geometry, migration, and evolution of wave orbital ripples at leo-15. J. Geophys. Res. Oceans 104, 1505–1524.
van Rijn, L., 2007. Unified View of Sediment Transport by Currents and Waves. i: Initiation of Motion.
Venditti, J.G., Church, M., Bennett, S.J., 2005. Morphodynamics of small-scale superimposed sand waves over migrating dune bed forms. Water resources research 41.
Wengrove, M., Foster, D., de Schipper, M., Lippmann, T., 2017. Wave and current ripple formation and migration during storms. Proc. Coast. Dyn. 955–965.
Wengrove, M., Foster, D., Lippmann, T., de Schipper, M., Calantoni, J., 2018. Observations of time-dependent bedform transformation in combined wave-current flows. J. Geophys. Res. Oceans 123, 7581–7598.
Wengrove, M., Foster, D., Lippmann, T., de Schipper, M., Calantoni, J., 2019. Observations of bedform migration and bedload sediment transport in combined wave-current flows. J. Geophys. Res. Oceans 124, 4572–4590.
Werner, B.T., 1999. Complexity in natural landform patterns. Science 284, 102–104.
Winter, C., Vittori, G., Ernstsen, V.B., Bartholdy, J., 2008. On the superimposition of bedforms in a tidal channel. In: Marine and River Dune Dynamics, pp. 337–344.